Plasmonics
https://doi.org/10.1007/s11468-019-00982-1

Optical Properties of Au-Doped Titanium Nitride Nanostructures: a Connection Between Density Functional Theory and Finite-Difference Time-Domain Method

Alireza Shabani[1,2] · Mehdi Khazaei Nezhad[2] · Neda Rahmani[1] · Mahmood Rezaee Roknabadi[2] · Mohammad Behdani[2] · Biplab Sanyal[1]

Received: 13 February 2019 / Accepted: 1 July 2019

Abstract
In this paper, we present a computational method to investigate optical properties of materials using a combination of density functional theory (DFT) calculations and finite-difference time-domain (FDTD) method. We show our method in the framework of an example for analyzing the effect of Au doping on optical transmission behavior of TiN compounds with a given geometry. First, DFT is employed based on generalized gradient approximation (GGA) exchange-correlation potential to investigate the electronic properties as well as dielectric function of TiN with respect to different percentages of doped Au. Our results reveal a growth in the imaginary part of dielectric function for energies below 4 eV by increasing Au doping level due to compression of $Ti_{1-x}Au_xN$ DOS into the Fermi energy. In order to clarify the impact of Au doping on the optical behavior of $Ti_{1-x}Au_xN$ with a given geometry, the optical dielectric function calculated from DFT was used as an input data for FDTD method to simulate a perforated surface plasmon system originated from $Ti_{1-x}Au_xN$-dielectric configuration via Optiwave package. It is observed that an increase in the Au level decreases the transmission intensity of excited modes of the perforated surface plasmon system, which is in agreement with the observed behavior for the imaginary part of dielectric function from DFT calculations. This implies that an enhanced imaginary part of dielectric function leads to more energy dissipation and finally less transmitted wave. The proposed method enables us to simulate optical properties of a wide range of compounds with arbitrary geometries and material-specific properties.

Keywords DFT calculations · FDTD method · Dielectric function · Energy dissipation · Optical transmission

Introduction

In recent years, numerous investigations were done to find new materials with prominent optical properties to replace the noble metals used nowadays. In the field of optics, most of the researches are focused on studying the impact of added material on optical properties of a given compound by means of experimental methods. They include a series of experimental-based studies from chemical or physical fabrication methods to optical characterization tools such as spectrophotometer to measure transmittance, reflectance, and absorbance of a compound, as the most significant quantities to assess the improvement of optical properties [1–4].

On the other hand, for materials with complex geometries, there are intensive limitations for experimental methods in synthesizing the desired structure. In order to overcome the problem, the studies focus on combining the experimental results with computational methods. This is done by using the response function of an engineered compound, measured by experimental technique [5–11], as an input data for computational methods such as finite-difference time-domain (FDTD) to calculate the optical spectra through solving the Maxwell equations for the proposed geometry.

The lack of a pure computational method, containing a series of consecutive theoretical processes, which allows us to simulate a wide range of compounds with arbitrary geometry in an easier way, is strongly felt. In the following, we introduce a theoretical study as a substitution to the aforementioned experimental and semi-experimental approaches, based

✉ Alireza Shabani
al.shabani@mail.um.ac.ir

[1] Department of Physics and Astronomy, Uppsala University, Box-516, 75120 Uppsala, Sweden

[2] Department of Physics, School of Science, Ferdowsi University of Mashhad, Mashhad 9177948974, Iran

Published online: 08 July 2019

on the combination of two powerful simulation techniques, the density functional theory (DFT) calculations and FDTD method, to make a connection between the optical response function and the optical transmission spectrum. We show the procedure in the form of an example for TiN compound. Our intention is to investigate the impact of Au doping on the optical behavior of a perforated surface plasmon system of TiN.

We deliberately chose the intermetallic TiN, because it seems to be a good candidate to demonstrate extraordinary optical behavior due to its plasmonic nature besides its unique mechanical and electrical properties [12–16]. Yet, most reports on the optical properties of TiN are limited to some experimental and theoretical studies, which contain conventional structures of TiN, including thin film, nanoparticles, and core-shell [17–20]. Therefore, more investigations are needed to explore the possibility of having useful optical features for arbitrary geometries.

This paper is divided into three main sections. The first part is devoted to the ab initio calculations of Au-doped TiN compound by using DFT, which includes simulation parameters and results and discussion for electronic and optical properties of this compound. In the second part, our method to make a connection between DFT and FDTD is described in detail, and the way to find required optical parameters of a material to introduce to the FDTD software is explained. In the last section, the DFT-simulated TiAuN compound is employed in the Optiwave FDTD software to calculate transmission behavior of the perforated surface plasmon system, with respect to different percentages of Au dopant.

DFT Calculations

Simulation Parameters

We investigate the electronic and optical properties of $Ti_{1-x}Au_xN$ compound using first-principle calculations. The SIESTA package was employed in the framework of Perdew-Burke-Ernzerhof (PBE) exchange-correlation functional within generalized gradient approximation (GGA) based on the linear combination of atomic orbital (LCAO) pseudopotential techniques. The integration in reciprocal space was performed over the *k*-point grid of 15 × 10 × 15 to describe an accurate ground state in a self-consistent calculation.

To simulate different percentages of Au doping in $Ti_{1-x}Au_xN$, we used a supercell with 16 Ti and N atoms (Fig. 1). To optimize the structures, the force on every atom was minimized to 0.002 eV/Å. Total energies were calculated with an accuracy of 10^{-4} eV. Also, the optical mesh of 50 × 50 × 50 was employed to calculate the optical dielectric function for an incident unpolarized electromagnetic wave.

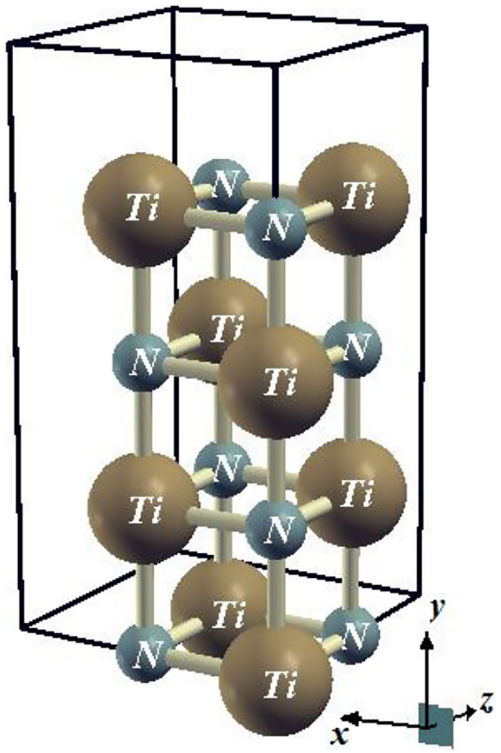

Fig. 1 The supercell of face-centered cubic (FCC) TiN containing 16 atoms (8 Ti and 8 N atoms)

Results and Discussion

At first, DFT was used to simulate pristine TiN with face-centered cubic (FCC) crystal structure. Then, Ti was substituted by Au to realize $Ti_{1-x}Au_xN$ compound with different percentages (x = 12.5 and 25). Figure 2 shows the electronic density of states for pure TiN along with 12.5 and 25% Au-doped TiN.

It is seen that Ti 3d state plays an important role in the conductivity of the TiN compound. This status can also be seen at higher concentrations of Au doping. In fact, the region around the Fermi energy (− 1.5 to 3.5 eV) is mainly occupied by Ti 3d state mixed with a few N 2p states. It contains filled states below and empty states above the Fermi energy which enable the electrons to make transition. In addition, the diagrams show the hybridization of Ti 3d and N 2p states in which the contribution of Au 5d state should be added as doping level is increasing. Our presented plot for TiN agrees well with the reported calculations [21–24].

It can be observed from Fig. 2b, c that the doping process causes two major effects on the DOS of TiN. First, by increasing the doping level, the DOS of Ti 3d state gradually decreases at energy interval of 2 to 3 eV and shifts to lower energy, as some small peaks are created above the Fermi energy up to 2 eV. It implies an increase in the number of discrete unoccupied states, which have the potential to host the excited electrons in the transition process.

Secondly, the DOS peak around − 5 eV energy, originated from hybridization of Ti 3d and N 2p, decreases and divides

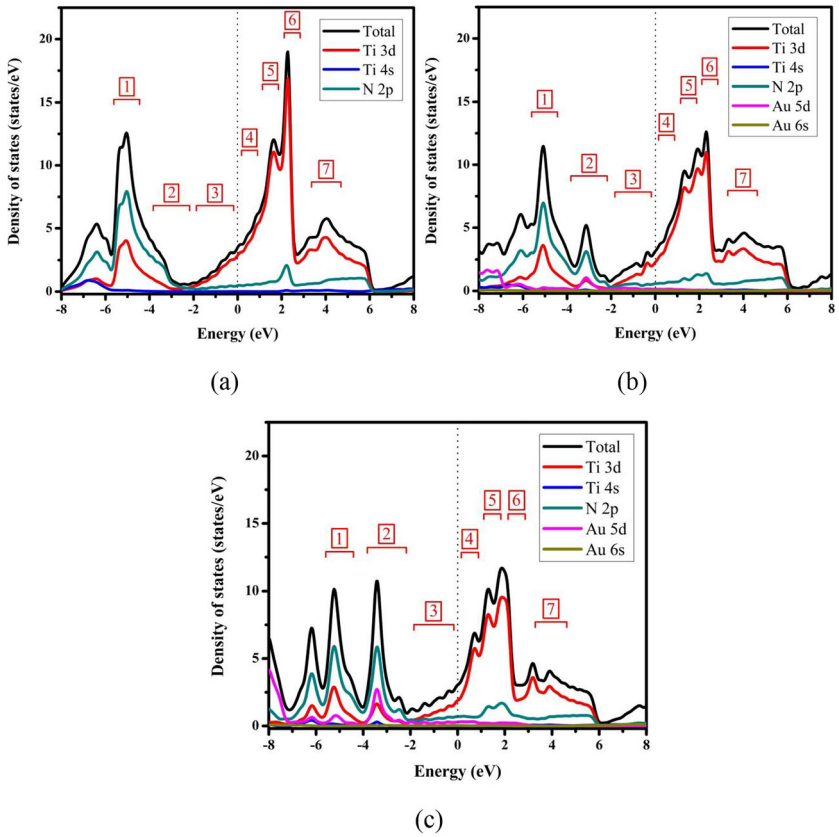

Fig. 2 Total and partial density of states of $Ti_{1-x}Au_xN$ for three values of x. **a** TiN. **b** $x = 0.125$. **c** $x = 0.25$

into two peaks by increasing Au dopant. In fact, participation of the Au 5d state in the orbital interactions caused the DOS peak around − 5 eV to decrease and the second DOS peak to appear at energy of − 3 eV. It is observed that by increasing the Au dopant, the peak height around − 3 eV becomes greater, being expected to play an important role in the optical behavior.

Hence, it can be concluded that the Au doping compressed states and pushed them towards the Fermi energy, which leads to an increase in the number of occupied and unoccupied states around the Fermi energy. Two mentioned phenomena cause a higher probability of electron transition at energy interval of 1 to 3 eV, which results in more energy loss in the optical region. In contrast, the states having shifted towards Fermi energy reduce the probability of electron transition at higher energies. This results in a decrease in the imaginary part of dielectric function for energy above 4 eV.

The optical behavior of a material can be directly explained through the dielectric function, which exhibits the response of materials to electromagnetic field. The imaginary part of dielectric function provides significant information about the optical loss and light absorption, while the real part shows the ability of material to respond in the form of dielectric polarization to the incident electromagnetic wave.

Figure 3 shows the imaginary part of dielectric function of $Ti_{1-x}Au_xN$ for three doping concentrations of Au ($x = 0$, 0.125 and 0.25). It is in good agreement with calculated results for TiN dielectric function by QUANTUM ESPRESSO and VASP packages, which were reported by other researchers [25, 26]. Since the transition of electron from lower to higher states corresponds to energy absorption, the energy difference between two peaks in the DOS is proportional to a particular peak in the imaginary part of dielectric function. In other words, the imaginary part of the dielectric function can be calculated from the momentum matrix elements between the occupied and unoccupied states in addition to the contribution of intraband transitions and is given by [27]:

$$\varepsilon_{\mathrm{img}}(\omega) = \varepsilon_{\mathrm{intra}} + \frac{Ve^2}{2\pi\hbar m^2\omega^2}\int d^3k \sum_{ij} \left|\langle K_i|P|K_j\rangle\right|^2 \times f(K_i)\left(1-f\left(K_j\right)\right)\delta\left(E_{K_i}-E_{K_j}-\hbar\omega\right), \quad (1)$$

where P is the electron momentum operator, $\hbar\omega$ is the energy of incident photon, and $|K_j\rangle$ and $|K_j\rangle$ denote filled initial state and empty final state, respectively.

DOS is divided into several domains in order to provide a clear insight on how the Au doping can affect the dielectric function and finally the optical properties of TiN compound. Moreover, since most contribution of electron transition is related to those electrons that are around the Fermi energy, only the energy intervals near the Fermi energy are specified here.

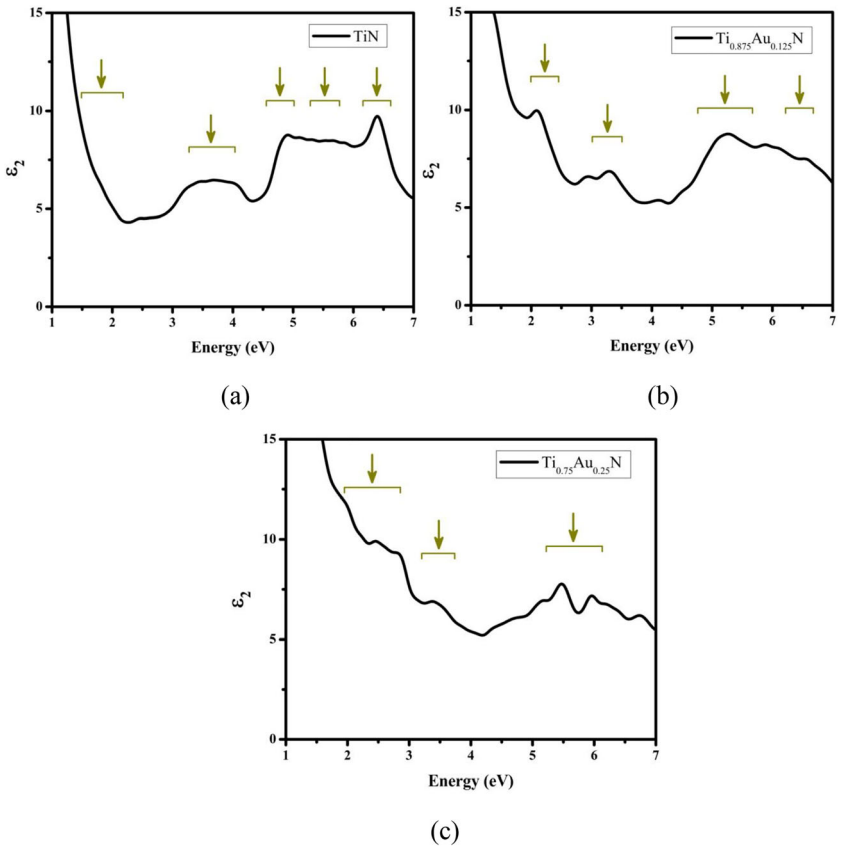

Fig. 3 The calculated imaginary part of dielectric functions for **a** TiN, **b** $Ti_{0.875}Au_{0.125}N$, and **c** $Ti_{0.75}Au_{0.25}N$ compounds. The arrows show the energies with the most possible electron transitions in the DOS

By comparing Figs. 2a and 3a, it is obvious that the peak ranged between 3 and 4 eV in the imaginary part of dielectric function stems from the electron transition from domain 3 with occupied state to the unoccupied domain 6 as well as transitions from domains 2 to 4 and 5 in the DOS diagram. Also, the peak between 4.5 and 5 eV mainly corresponds to the transitions from 1 to 4, 2 to 5, and 3 to 7. For higher energy peaks in the imaginary part of dielectric function, electron transitions in further domains should be considered. For instance, the flat domain that ranged between 5 and 6 eV is ascribed to the transition from domains 1 to 5, 2 to 6, and 3 to 7. What is more, the sharp peak around 6.5 eV corresponds to the transitions from 2 to 6 and 7 and 1 to 5. It should be noted that the DOS above domain 7 has the least contribution in electron transition because of its small amount.

As mentioned before, by doping Au atom in the TiN, the DOS of domain 6 reduces as some states are created above the Fermi level in domains 4 and 5, which is expected to play an important role in the energy loss of incident beam due to raising the probability of interband transitions. For $x = 0.125$, transitions from domains 3 to 4 and 5 increase that lead to a growth in the imaginary part of dielectric function at energy range of 1.5 to 2.5 eV. It can also be seen that the peak ranged between 3 and 4.5 eV for the TiN dielectric function (see Fig. 3a) shifts to lower energy (3 and 3.5 eV) in the case of 12.5% Au-doped TiN (see Fig. 3b). This is due to the creation of a new peak in the second domain of DOS, facilitating electron transitions between domains 2 and 4 with lower energy compared to the pure TiN case. Moreover, a decrease in the imaginary part of dielectric function is seen for the 12.5% Au-doped TiN at energy range of 4.5 to 7 eV, which is attributed to the reduced DOS peak in the domains 1 and 6. This effect can be obviously observed by the eliminated peak around 6.5 eV for the dielectric function of $Ti_{0.875}Au_{0.125}N$ in comparison to pure TiN.

By increasing the concentration of Au atom to $x = 0.25$, the dielectric function of $Ti_{0.75}Au_{0.25}N$ undergoes significant changes as it is more sensible in comparison to $Ti_{0.875}Au_{0.125}N$. The imaginary part of dielectric function increases at energies less than 4 eV, especially at energy range of 2 to 3 eV and 3to 3.5 eV due to more electron transitions in the DOS diagram from domains 3 to 4 and 5 and 2 to 4, respectively (see Fig. 3c). Adding more Au atoms intensified two mentioned effects, comprising a decrease in DOS of domains 1 and 6 and an increase in DOS of domains 2, 4, and 5. Regarding the states having been pushed towards the Fermi level, it is reasonable to see a greater amount of dielectric function for energies between 2 and 3 eV and 3 and 3.5 eV. In contrast, there is a decrease in the dielectric function of $Ti_{0.75}Au_{0.25}N$ for energies greater than 4 eV compared to $Ti_{0.875}Au_{0.125}N$, which is attributed to diminished DOS in the domains 1 and 6. The point that should be noted is to consider the optical selection rules in all possible transitions.

As a result, by increasing the doping level of Au atom in the TiN compound, the imaginary part of dielectric function is divided into two parts in terms of the frequency of incident beam. For energies less than 4 eV, the amount of dielectric function grows that shows an increase in the energy dissipation of interacting light, while it decreases above 4 eV, which is proportional to less energy dissipation. It implies that the substitution of Au element in the TiN compound leads to an improvement in the optical response within the UV region.

Connection Between DFT and FDTD

After evaluating the optical behavior of $Ti_{1-x}Au_xN$ for different levels of Au doping by ab initio calculations, the next section is devoted to demonstrating a straight example that provides a clear view on how the Au doping can affect the optical behavior of $Ti_{1-x}Au_xN$ compound with a given geometry. In fact, the following section is focused on investigating the effects of atomic substitution on the optical transmission spectrum of a surface plasmon polariton system, containing periodic arrays of holes, via Optiwave package, where the connection between DFT calculations and FDTD method occurs as the main aim of this research.

To start the simulation, it is needed to define the optical behavior of proposed compounds through specifying their main optical parameters. The Drude-Lorentz model, which shows the response of dispersive materials to the electromagnetic field, is employed to interpret the imaginary part of dielectric function. The frequency-dependent Drude-Lorentz dielectric function is given by:

$$\varepsilon(\omega) = \varepsilon_\infty + \sum_j \frac{f_j \omega_p^2}{\left(\omega_j^2 - \omega^2\right) - i\omega\gamma_j}, \tag{2}$$

where ω_j, γ_j, and f_j are frequency-independent oscillator resonance frequencies, bandwidths, and oscillator strengths, respectively. The background permittivity is described by ε_∞, and ω_p is the plasma frequency.

The Drude-Lorentz model was selected because it is more matched with experimental data in comparison to other models. It contains Drude's free electron model for metals in low-frequency ranges as well as the contribution of interband transitions. These transitions dissipate the energy of incident beam, which appears in the form of some peaks in the imaginary part of dielectric function. Each individual peak is modeled by an oscillator that absorbs the electromagnetic field thorough resonance. Required parameters to define the optical behavior of a matter, such as number, strength, and damping coefficient of oscillators can be achieved through fitting the Lorentzian peaks to the imaginary part of dielectric function.

Figure 4 depicts the Lorentzian peaks fitted to the imaginary part of dielectric function of $Ti_{1-x}Au_xN$ for three values

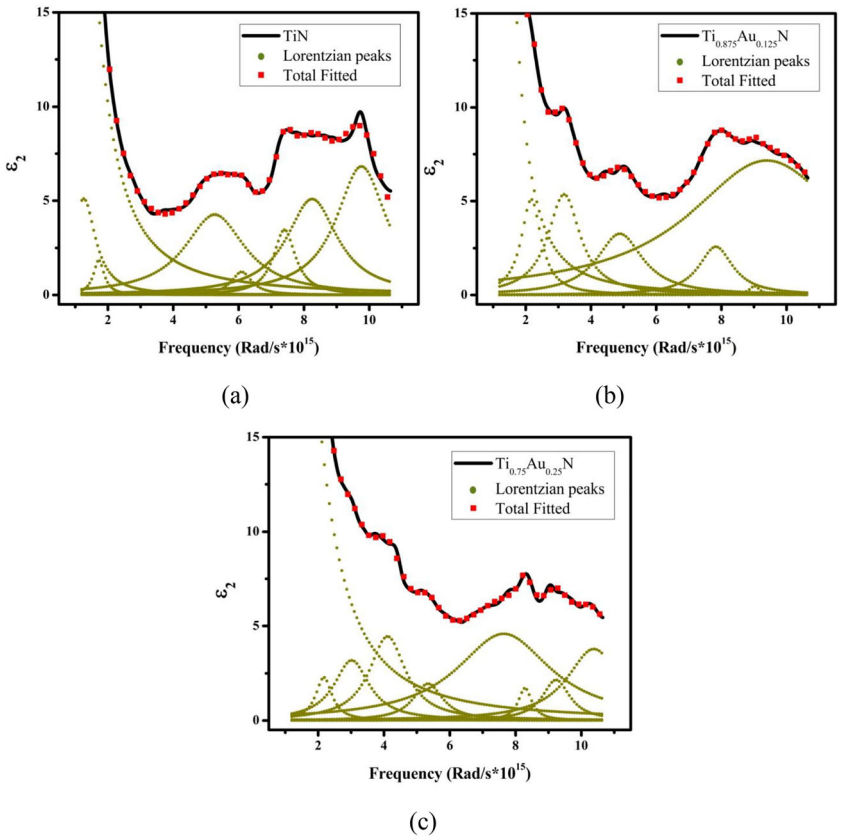

Fig. 4 The different components of Lorentzian peaks (dotted dark yellow line) fitted on the imaginary part of dielectric function (solid black line) for three values of Au-doped in $Ti_{1-x}Au_xN$. **a** $x = 0$. **b** $x = 0.125$. **c** $x = 0.25$

of Au concentrations ($x = 0$, 0.125, and 0.25). Since the input data in the Optiwave package are frequency-dependent, the dielectric permittivity is turned to a function of frequency.

To enhance the precision of fitted curves, we used 9, 8, and 10 Lorentzian peaks for $Ti_{1-x}Au_xN$ with $x = 0$, 0.125, and 0.25, respectively. The plasmon frequency (ω_p) was also calculated by DFT method, being 9.47, 6.92, and 8.72×10^{15} rad/s for $x = 0$, 0.125, and 0.25, respectively. As it is clear, the fitted curve in each diagram (red square) is highly matched with the corresponding imaginary part of dielectric function (black solid line). This helps us to accurately simulate the optical properties of any geometry. The fitting parameters of each compound are listed in the Tables 1, 2, and 3.

FDTD Simulations

To investigate transmission behavior of the perforated surface plasmon system of $Ti_{1-x}Au_xN$, the finite-differential time-domain (FDTD) method was employed via the Optiwave package. At first, a two-dimensional system, containing the $Ti_{1-x}Au_xN$ film with square subwavelength holes within, was simulated on the top of a dielectric layer with a refractive index of $n = 2$ (shown in Fig. 5). The thickness of the $Ti_{1-x}Au_xN$ film and dielectric layer was 20 and 50 nm, respectively. Also, the size of square holes was the same (shown by *S*), and the periodic lattice constant was identical for both *x* and *y* directions (shown by *a*), which is defined as the separation distance between two successive holes.

Since the system was placed in the *x*-*y* plane, the periodic boundary condition (PBC) was applied in the *x*- and *y*-directions, and the absorbing perfectly matched layer (APML) was considered in the *z*-direction. A 30° polarized continuous Gaussian input electromagnetic wave with time offset 4e −15 s and half width 0.8e−15 s was selected, which propagated along the *z*-direction. Mesh size of 4 nm along the *x*-, *y*-, and *z*-directions was used. The aim of employing the FDTD method is to solve Maxwell equations in order to obtain the spatial and temporal dependency of the electromagnetic waves in each point. The process is done by applying boundary conditions to the simplified discrete equations originated from derivation formula.

$Ti_{1-x}Au_xN$ is an intermetallic compound thus, it is expected to show the surface plasmon polariton (SPP) properties resulting from the coupling of the electromagnetic wave with the electron sea at the metal-dielectric interface. The electrons mimic the propagating component of electromagnetic wave at $Ti_{1-x}Au_xN$-dielctric interface and collectively oscillate on the *x*-*y* plane, which is known as the SPP effect. Such phenomenon is expected to strongly influence the optical behavior through absorbing the electromagnetic field by electrons and reemitting it by oscillating charged particle mechanism.

By creating ordered arrays of subwavelength holes within the $Ti_{1-x}Au_xN$ film, other phenomena appear which directly affect the optical transmission of the proposed structure. First, the interaction between incident electromagnetic field and collected electrons at sharp edges and tips leads to the creation of local surface plasmon resonance (LSPR) as shown in Fig. 6b. The LSPR indicates a collective movement of electrons which

Table 1 The characteristics of the Lorentzian oscillators containing the resonance frequencies, oscillation strength, and damping coefficient for TiN

Resonance	ω_j (10^{15} rad/s)	γ_j (10^{15} rad/s)	f_j
1	0	0.304	1
2	0.653	1.06	0.586
3	1.261	0.875	0.063
4	1.723	0.402	0.014
5	5.272	2.260	0.567
6	6.094	0.756	0.063
7	7.404	0.819	0.234
8	8.250	1.916	0.896
9	9.760	1.883	1.400

Table 2 The characteristics of the Lorentzian oscillators containing the resonance frequencies, oscillation strength, and damping coefficient for $Ti_{0.875}Au_{0.125}N$

Resonance	ω_j (10^{15} rad/s)	γ_j (10^{15} rad/s)	f_j
1	0	0.026	1
2	1.112	0.892	0.881
3	2.170	0.747	0.172
4	3.176	1.209	0.429
5	4.887	1.715	0.573
6	7.832	1.277	0.539
7	9.017	0.407	0.036
8	9.394	5.866	8.242

Table 3 The characteristics of the Lorentzian oscillators containing the resonance frequencies, oscillation strength, and damping coefficient for $Ti_{0.75}Au_{0.25}N$

Resonance	ω_j (10^{15} rad/s)	γ_j (10^{15} rad/s)	f_j
1	0	0.025	1
2	0.799	1.506	0.942
3	2.174	0.604	0.039
4	3.019	1.308	0.166
5	4.109	1.341	0.323
6	5.341	1.091	0.150
7	7.642	3.497	1.615
8	8.289	0.507	0.095
9	9.231	1.020	0.267
10	10.378	1.983	1.026

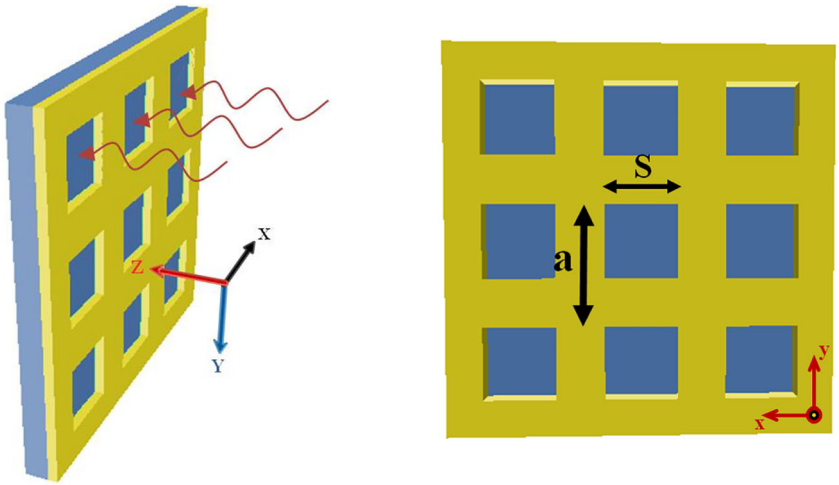

Fig. 5 Schematic picture of simulated square array of holes within the $Ti_{1-x}Au_xN$ thin film on the dielectric substrate. *a* indicates the lattice constant and *S* is the hole size. The thickness of the $Ti_{1-x}Au_xN$ film and dielectric layer are 20 and 50 nm, respectively

is restricted to the nanometer dimensions of sharp edges and tips. The LSPR is known as the origin of hot spots in the field distribution pattern that enhances the intensity of transmitted beam [28]. Second, another effect is directly related to the holes and their dimensions. They play a role similar to waveguides in transmitting the electromagnetic field, depending on the hole dimension [29].

On the other hand, the existence of periodic arrays of square holes inside the $Ti_{1-x}Au_xN$ film is equal to a two-dimensional grating system with the same lattice constant in both directions. It causes the transmission spectrum to divide to several resonance peaks. Each individual peak indicates a particular mode of excited surface plasmon resonance wavelength which is given by [30]:

$$\lambda_{sp} = \frac{a}{\sqrt{n^2 + m^2}} \sqrt{\frac{\varepsilon_d \varepsilon_m}{\varepsilon_d + \varepsilon_m}}, \tag{3}$$

where λ_{sp} is the wavelength of the excited surface plasmon mode, a is the periodic constant of the hole array, (n, m) pair denotes the mode's order, and ε_m and ε_d are the response functions of the metal and dielectric layers, respectively.

Figure 6 shows the transmission spectrum of $Ti_{1-x}Au_xN$-dielectric configuration for different doping concentrations of Au ($x = 0$, 0.125, and 0.25). One can clearly see the different orders of excited surface plasmon modes of the system from the plot. It is obvious that an extraordinary optical transmission (EOT) occurred at $\lambda = 970$ nm, which is a characteristic of these types of structures. As was previously mentioned in the literature, the place of the EOT peak is directly dependent on the geometrical parameters of the configuration, since by increasing the Au doping level, it does not change [28]. It is observed that pure TiN has the most optical transmission spectrum in comparison to Au-doped TiN. By increasing the doping level, the transmission approximately decreases 10% around the EOT peak and more than 20% in the visible region. This decrease essentially stems from the imaginary part of the dielectric function, which connects the optical behavior to structures. By comparing the imaginary part of dielectric function for three various percentages of the Au atom in $Ti_{1-x}Au_xN$ alloys (see Fig. 3), it becomes clear that the imaginary part of dielectric function has an inverse relation with the intensity of transmitted spectrum.

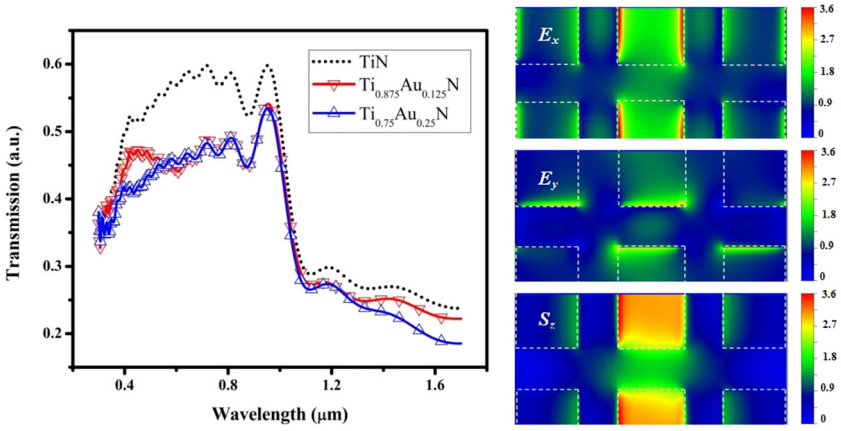

(a) (b)

Fig. 6 **a** The calculated optical transmission spectrum of the orderly perforated $Ti_{1-x}Au_xN$-dielectric system for different doping concentrations of Au. **b** The electric field distribution (E_x and E_y) accompanied with S_z at $\lambda = 970$ nm. The dashed lines show square holes within the $Ti_{1-x}Au_xN$ layer. The LSPR and waveguide mode are clearly observed in this picture

More amount of dielectric function leads to lower transmission, which indicates more energy dissipation and vice versa. In fact, the interband transitions, which are accompanied with energy absorption, are responsible for the dissipation.

Furthermore, it can be seen that the intensity of the transmitted beam for $Ti_{0.875}Au_{0.125}N$ is slightly more than $Ti_{0.75}Au_{0.25}N$ in all Vis-IR regions. This is consistent with the results shown in Fig. 3 for the imaginary part of dielectric functions. Since the dielectric function of $Ti_{0.75}Au_{0.25}N$ is more than $Ti_{0.875}Au_{0.125}N$ for all energies below 4 eV, it is expected that the $Ti_{0.75}Au_{0.25}N$ will show more energy dissipation in comparison with $Ti_{0.875}Au_{0.125}N$. Based on this reasoning, there should be an enhancement in the optical transmission spectrum for energies above 4 eV by replacing the Au atom with Ti in the TiN compound, because increasing the doping level up to 25% causes the dielectric function to reach its lowest amount in the case of $Ti_{0.75}Au_{0.25}N$. In addition, the transmission of all three compounds reaches to the same amount at $\lambda = 400$ nm, which is considered a starting point for optical enhancement. Nevertheless, unfortunately, due to software limitations in short wavelengths, we are unable to show this effect.

Conclusion

In this paper, we introduced a new method to evaluate optical properties of materials by combining first-principle calculations and finite-difference time-domain method. We presented it by studying the effect of Au doping on the optical behavior of TiN in an orderly perforated surface Plasmon system. At first, density functional theory was employed within generalized gradient approximation to calculate the electronic density of states and optical dielectric functions of $Ti_{1-x}Au_xN$ for three concentrations of Au dopant: $x = 0$, 0.125, and 0.25. Then, the imaginary part of dielectric function, obtained from DFT calculations, was used as an input data for the Optiwave package to simulate a surface plasmon system which contains a two-dimensional $Ti_{1-x}Au_xN$ film, comprising periodic arrays of square subwavelength holes, on top of a dielectric layer. The simulations revealed a decrease in the optical transmission spectrum in the Vis-IR regions for $x =$ 0.125 and 0.25, which was attributed to the increased interband transitions reflected in the imaginary part of dielectric function at corresponding frequency domains. This method shows to have potential in applying to wide ranges of material to evaluate their optical properties in arbitrary geometries.

References

1. Park TY, Choi YS, Kang JW, Jeong JH, Park SJ, Jeon DM, Kim JW, Kim YC (2010) Enhanced optical power and low forward voltage of GaN-based light-emitting diodes with Ga-doped ZnO transparent conducting layer. Appl Phys Lett 96:051124
2. Xi JQ, Schubert MF, Kim JK, Schubert EF, Chen M, Lin SY, Liu W, Smart JA (2007) Optical thin-film materials with low refractive index for broadband elimination of Fresnel reflection. Nat Photonics 1:176–179
3. Huang YF, Chattopadhyay S, Jen YJ, Peng CY, Liu TA, Hsu YK, Pan CL, Lo HC, Hsu CH, Chang YH, Lee CS (2007) Improved broadband and quasi-omnidirectional anti-reflection properties with biomimetic silicon nanostructures. Nat Nanotechnol 2:770–774
4. Singh P, Sharma P, Sharma V, Thakur A (2017) Linear and nonlinear optical properties of Ag-doped Ge2Sb2Te5 thin films estimated by single transmission spectra. Semicond Sci Technol 32: 045015
5. Tang B, Li Z, Liu Z, Callewaert F, Aydin K (2016) Broadband asymmetric light transmission through tapered metallic gratings at visible frequencies. Sci Rep 6:39166
6. Lehr D, Reinhold J, Thiele I, Hartung H, Dietrich K, Menzel C, Pertsch T, Kley E, Tünnermann A (2015) Enhancing second harmonic generation in gold nanoring resonators filled with lithium niobate. Nano Lett 15:1025–1030
7. Lassiter JB, Sobhani H, Fan JA, Kundu J, Capasso F, Nordlander P, Halas NJ (2010) Fano resonances in plasmonic nanoclusters: geometrical and chemical tenability. Nano Lett 10:3184–3189
8. Hu L, Chen G (2007) Analysis of optical absorption in silicon nanowire arrays for photovoltaic applications. Nano Lett 7:3249–3252
9. Rodrigo SG, García-Vidal FJ, Martín-Moreno L (2008) Influence of material properties on extraordinary optical transmission through hole arrays. Phys Rev B 77:075401
10. Liu N, Mesch M, Weiss T, Hentschel M, Giessen H (2010) Infrared perfect absorber and its application as plasmonic sensor. Nano Lett 10:2342–2348
11. Huo D, Zhang J, Wang H, Ren X, Wang C, Su H, Zhao H (2017) Broadband perfect absorber with monolayer MoS_2 and hexagonal titanium nitride nano-disk array. Nanoscale Res Lett 12(465)
12. Recco A, Lopez D, Bevilacqua AF, da Silva F, Tschiptschin AP (2007) Improvement of the slurry erosion resistance of an austenitic stainless steel with combinations of surface treatments: nitriding and TiN coating. Surf Coat Technol 202:993–997
13. Wittmer M, Studer B, Melchior H (1981) Electrical characteristics of TiN contacts to N silicon. J Appl Phys 52:5722–5726
14. Patsalas P, Charitidis C, Logothetidis S, Dimitriadis CA, Valassiades O (1999) Combined electrical and mechanical properties of titanium nitride thin films as metallization materials. J Appl Phys 86:5296–5298
15. Guler U, Shalaev VM, Boltasseva A (2015) Nanoparticle plasmonics: going practical with transition metal nitrides. Mater Today 18:227–237
16. Guler U, Naik GV, Boltasseva A, Shalaev VM, Kildishev AV (2012) Performance analysis of nitride alternative plasmonic materials for localized surface plasmon applications. Appl Phys B Lasers Opt 107:285–291
17. Cortie MB, Giddings J, Dowd A (2010) Optical properties and plasmon resonances of titanium nitride nanostructures. Nanotechnology 21:115201
18. Kim J, Jhi SH, Lee Ryeol K (2011) Color of TiN and ZrN from first-principles calculations. J Appl Phys 110:083501
19. Reinholdt A, Pecenka R, Pinchuk A, Runte S, Stepanov AL, Weirich TE, Kreibig U (2004) Structural, compositional, optical and colorimetric characterization of TiN-nanoparticles. Eur Phys J D 31:69–76
20. Lalisse A, Tessier G, Plain J, Baffou G (2016) Plasmonic efficiencies of nanoparticles made of metal nitrides (TiN, ZrN) compared with gold. Sci Rep 6:38647

21. Matenoglou GM, Lekka CE, Koutsokeras LE, Karras G, Kosmidis C, Evangelakis GA, Patsalas P (2009) Structure and electronic properties of conducting, ternary $Ti_xTa_{1-x}N$ films. J Appl Phys 105:103714
22. Marlo M, Milman V (2000) Density-functional study of bulk and surface properties of titanium nitride using different exchange-correlation functional. Phys Rev B 62:2899–2907
23. Yang Y, Lu H, Yu C, Chen JM (2009) First-principles calculations of mechanical properties of TiC and TiN. J Alloys Compd 485: 542–547
24. Yu S, Zeng Q, Oganov AR, Frapper G, Zhang L (2015) Phase stability, chemical bonding and mechanical properties of titanium nitrides: a first-principles study. Phys Chem Chem Phys 17:11763–11769
25. Kim J, Jhi SH, Ryeol Lee K (2011) Color of TiN and ZrN from first-principles calculations. J Appl Phys 110:083501
26. Catellani A, Calzolari A (2017) Plasmonic properties of refractory titanium nitride. Phys Rev B 95:115145
27. Liu K, Fan H, Ren P, Yang C (2011) Structural, electronic and optical properties of BiFeO3 studied by first-principles. J Alloys Compd 509:1901–1905
28. Shabani A, Rezaei Roknabadi M, Behdani M, Kazaei Nezhad M, Rahmani N (2017) Extraordinary optical transmission of periodic array of subwavelength holes within titanium nitride thin film. J Nanophotonics 11:036006
29. Jin EX, Xu X (2006) Plasmonic effects in near-field optical transmission enhancement through a single bowtie-shaped aperture. Appl Phys B Lasers Opt 84:3–9
30. Ruan Z, Qiu M (2006) Enhanced transmission through periodic arrays of subwavelength holes: the role of localized waveguide resonances. Phys Rev Lett 96:233901